# Biodegradable synthetic high-density lipoprotein nanoparticles for atherosclerosis

Sean Marrache[a] and Shanta Dhar[a,b,1]

[a]NanoTherapeutics Research Laboratory, Department of Chemistry, and [b]Department of Physiology and Pharmacology, University of Georgia, Athens, GA 30602

Edited by Robert Langer, Massachusetts Institute of Technology, Cambridge, MA, and approved April 15, 2013 (received for review January 29, 2013)

**Atherosclerosis remains one of the most common causes of death in the United States and throughout the world because of the lack of early detection. Macrophage apoptosis is a major contributor to the instability of atherosclerotic lesions. Development of an apoptosis targeted high-density lipoprotein (HDL)-mimicking nanoparticle (NP) to carry contrast agents for early detection of vulnerable plaques and the initiation of preventative therapies that exploit the vascular protective effects of HDL can be attractive for atherosclerosis. Here, we report the construction of a synthetic, biodegradable HDL-NP platform for detection of vulnerable plaques by targeting the collapse of mitochondrial membrane potential that occurs during apoptosis. This HDL mimic contains a core of biodegradable poly(lactic-*co*-glycolic acid), cholesteryl oleate, and a phospholipid bilayer coat that is decorated with triphenylphosphonium (TPP) cations for detection of mitochondrial membrane potential collapse. The lipid layer provides the surface for adsorption of apolipoprotein (apo) A-I mimetic 4F peptide, and the core contains diagnostically active quantum dots (QDs) for optical imaging. In vitro uptake, detection of apoptosis, and cholesterol binding studies indicated promising detection ability and therapeutic potential of TPP-HDL-apoA-I-QD NPs. In vitro studies indicated the potential of these NPs in reverse cholesterol transport. In vivo biodistribution and pharmacokinetics indicated favorable tissue distribution, controlled pharmacokinetic parameters, and significant triglyceride reduction for i.v.-injected TPP-HDL-apoA-I-QD NPs in rats. These HDL NPs demonstrate excellent biocompatibility, stability, nontoxic, and nonimmunogenic properties, which prove to be promising for future translation in early plaque diagnosis and might find applications to prevent vulnerable plaque progression.**

coronary heart disease | diabetes | good cholesterol | atheroprotection | obesity

Despite advances in both primary and secondary prevention, atherosclerosis (1) remains one of the leading causes of morbidity and mortality in the Western world because of the lack of early detection and targeted therapy. In general, atherosclerosis is a result of excess cholesterol circulating in the bloodstream. At the cellular level, atherosclerotic plaque formation is caused by cholesterol consumption and foam cell formation by macrophages situated within the intimal layers of the arteries (2). The term "vulnerable plaque" designates a plaque at high risk of disruption leading to thrombosis. Identification of vulnerable plaques before the thrombus formation is essential to enable the development of treatment modalities. One intriguing possibility for the development of image-guided therapies of coronary heart diseases (CHDs) is through high-density lipoproteins (HDLs), because of its function in the reverse cholesterol transport (RCT) pathway (3, 4). Along with apolipoprotein (apo) E, which promotes cholesterol efflux from foam cells, apoA-I–containing HDL facilitate the transport of cholesterol from lesions. Development of targeted HDL nanoparticles (NPs) to carry contrast agents for early detection of vulnerable plaques (5) and the initiation of preventative therapies that exploit the vascular protective effects of HDL could reduce the morbidity and mortality of thromboembolism (6). It is hypothesized that apoptosis of macrophages and of smooth muscle cells (SMCs) play an important role in plaque rupture (7). A unique approach for the noninvasive detection of apoptosis in SMCs and macrophages could be developed by targeting the collapse of the mitochondrial membrane potential ($\Delta\Psi_m$), a hallmark of the initiating phase of apoptosis (8). Thus, a completely synthetic biodegradable $\Delta\Psi_m$ targeting HDL mimicking NP containing contrast agents could be of enormous benefits to patients with CHD. Surprisingly, all of the reports on using HDL NPs for imaging atherosclerosis are based on reconstituted HDL (rHDL) (9–11) (*SI Appendix*, Table S1). Particles based on rHDL use lipoproteins and apoA-I extracted from human plasma. A potential problem in using rHDL NPs includes batch-to-batch variability when lipoproteins are isolated from donor plasma and scale-up challenges. A completely synthetic targeted HDL-mimicking NP platform that can navigate through the interstitial space protecting its contrast agent to the mitochondria of apoptotic macrophages in vulnerable plaque would result in potential early detection of atherosclerotic plaques.

There are a handful of HDL-mimicking liposomes and metal-based carriers for targeted delivery of siRNA, therapeutics, or contrast agents for cancer therapy (12–16) (*SI Appendix*, Table S1). However, no example thus far demonstrates the use of the Food and Drug Administration (FDA)-approved biodegradable poly(lactic-*co*-glycolic acid) (PLGA)-based synthetic HDL NPs. In this report, we present a proof-of-concept demonstration of such a technology. We developed a fluorescent HDL-mimicking polymer lipid NP platform (Fig. 1) consisting of a HDL resembling hydrophobic core of PLGA and cholesteryl oleate (CO). The polymer-cholesterol matrix incorporated diagnostically active quantum dot (QD)-conjugated polymer PLGA-block (*b*)-polyethylene glycol (PEG), PLGA-*b*-PEG-QD for optical imaging. This core is surrounded by a 1,2-distearoyl-*sn*-glycero-3-phosphoethanolamine (DSPE)-PEG-COOH lipid layer embedded with cholesterol and apoA-I mimetic 4F peptide with a FAE-KFKEAVKDYFAKFWD sequence (13), and a triphenyl phosphonium (TPP) cation containing stearyl-TPP ligand for targeting the collapse of $\Delta\psi_m$ during apoptotic events. Lipophilic TPP cations are known to accumulate several hundredfold by mitochondria within cells and can be used to direct a range of probe or therapeutic molecules to the mitochondria (17). Here, we report our preliminary results demonstrating the ability to construct such a biodegradable HDL mimic, in vitro and in vivo execution of this platform for detection, and therapy of vulnerable plaques.

## Results and Discussion

**Development of Synthetic HDL-Mimicking NPs.** Clinical uses of PLGA, PEG, and lipids in FDA-approved products motivated us to use these components to engineer completely synthetic HDL-mimicking polymer lipid hybrid NPs with the ability of high contrast agent loading for utilization of cardioprotective action

Author contributions: S.D. designed research; S.M. performed research; S.M. contributed new reagents/analytic tools; S.M. and S.D. analyzed data; and S.D. wrote the paper.

The authors declare no conflict of interest.

This article is a PNAS Direct Submission.

[1]To whom correspondence should be addressed. E-mail: shanta@uga.edu.

This article contains supporting information online at www.pnas.org/lookup/suppl/doi:10.1073/pnas.1301929110/-/DCSupplemental.

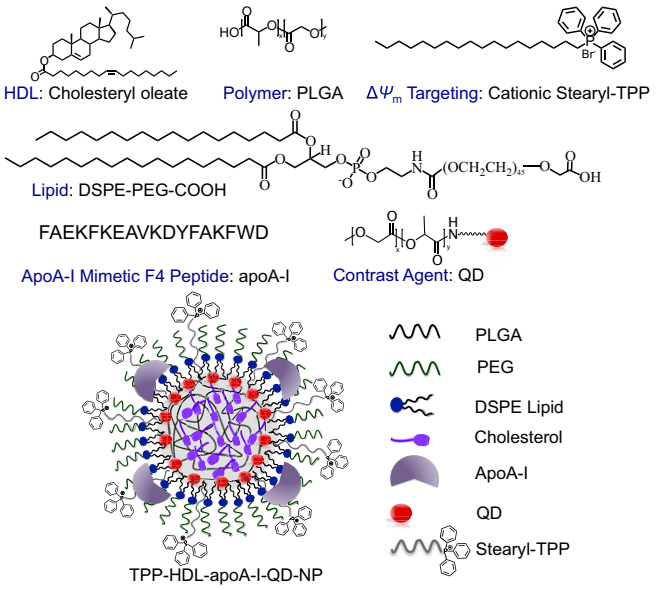


**Fig. 1.** Schematic diagram of the mitochondria-targeted biodegradable HDL mimicking NP platform and various components.

of HDL. A HDL-mimicking hybrid NP with a cholesterol and PLGA core was synthesized via self-assembly of PLGA, PLGA-*b*-PEG-QD, CO, cationic stearyl-TPP (*SI Appendix*, Fig. S1–S3), DSPE-PEG-COOH, and apoA-I mimetic peptide through a two-step modified nanoprecipitation method (*SI Appendix*, Fig. S4). For the nontargeted NPs, polyvinyl alcohol (PVA) was used instead of stearyl-TPP. Dynamic light scattering (DLS) measurements revealed the size of the mitochondria-targeted NPs, TPP-HDL-apoA-I-QD NPs to be ~123 ± 3 nm and are monodispersed (Fig. 2 and *SI Appendix*, Fig. S5 and Table S2). This small size of the targeted NPs will facilitate extravasation in areas with enhanced endothelial permeability, such as atherosclerotic lesions. The size of nontargeted HDL-apoA-I-QD NPs by DLS was found to be ~191 ± 7 nm. The hydrodynamic radius of the targeted NPs determined by DLS agrees with the transmission electron microscopy (TEM) results; however, for the nontargeted NPs, the hydrodynamic radius determined by DLS is almost twice the TEM size. We believe that this difference is due to the size variation of the lipid layers between targeted and nontargeted NPs and the location of the QDs within the core. The stearyl TPP in the targeted NPs has a molecular weight of ~500, whereas PVA in the nontargeted NPs has an average molecular weight range of 10,000–26,000. The QDs are located at the interface between the core and lipid layer. Therefore, by the unstained TEM images as reported here, the particles appear to be of same size for the targeted NPs. For the nontargeted NPs, DLS takes into account the larger lipid layer rendering them bigger compared with TEM size. Zeta potential measurements showed that the mitochondria targeted NPs are highly positively charged (~39 mV) (Fig. 2 and *SI Appendix*, Fig. S6 and Table S2). Our recent study indicated that a NP size of <160 nm and zeta potential of ~30 mV is an optimized formulation for mitochondria targeting (18). The nontargeted NP surface is negatively charged (~−28 mV). Composition analysis of the targeted NPs by inductively coupled plasma mass spectrometry (ICP-MS) for QD indicated 70% QD encapsulation efficiency (EE) and the nontargeted NPs showed moderately higher EE of ~83% (*SI Appendix*, Table S3). A major challenge of atherosclerosis imaging is the design of imaging probes to achieve sufficient target-to-background levels for visualization and high loading of the contrast agent to boost the signal at the target. A high QD incorporation as observed in our NPs might face less challenge when executed in vivo. Spectroscopic analysis of targeted and nontargeted NPs for quantification of apoA-I by examining tryptophan absorbance at 280 nm showed that the percent loading varies between 1.7 and 2%. Cholesterol analysis of NPs using Amplex Red assay demonstrated ~58% cholesterol loading (*SI Appendix*, Table S3). An interesting observation was that cholesterol and apoA-I loadings do not change significantly with formulation that might be indicative that this synthetic HDL tries to attain a specific cholesteryl ester (CE):apoA-I ratio (*SI Appendix*, Table S3) as seen in native HDL particles (19).

**Stability, Toxicity, and Immunogenic Properties of HDL-Mimicking NPs.** In addition to the size, charge, and contrast agent loading, serum stability and immunological effects of these unique NPs are expected to affect the in vivo biodistribution (bioD), pharmacokinetic (PK) parameters, and overall utility of this system. In vitro serum stability of the NPs was investigated by storing a 2.5 mg/mL NP suspension in 10% (vol/vol) fetal bovine serum (FBS)-Dulbecco's modified Eagle medium (DMEM) at 4 °C, room temperature (RT), and 37 °C and monitoring the changes in particle size and surface charge. Serum proteins showed no significant effect on the size, polydispersity index (PDI), and surface charge of the targeted NPs over a period of 7 d at all three temperatures (*SI Appendix*, Fig. S7). These results are indicative of an excellent stability of the targeted NPs under biologically relevant conditions. For in vivo studies, especially when positively charged NPs are injected at multiple time points, the potential exists for an immunogenic reaction that could adversely affect the binding of the NPs to the intended target or, even worse, be unsafe. We focused on macrophage-associated immune responses from the targeted and nontargeted HDL NPs by measuring the production of cytokines interleukin 6 (IL-6) and tumor necrosis factor α (TNF-α) by using an enzyme-linked immunosorbent assay (ELISA). Lipopolysaccharide (LPS)

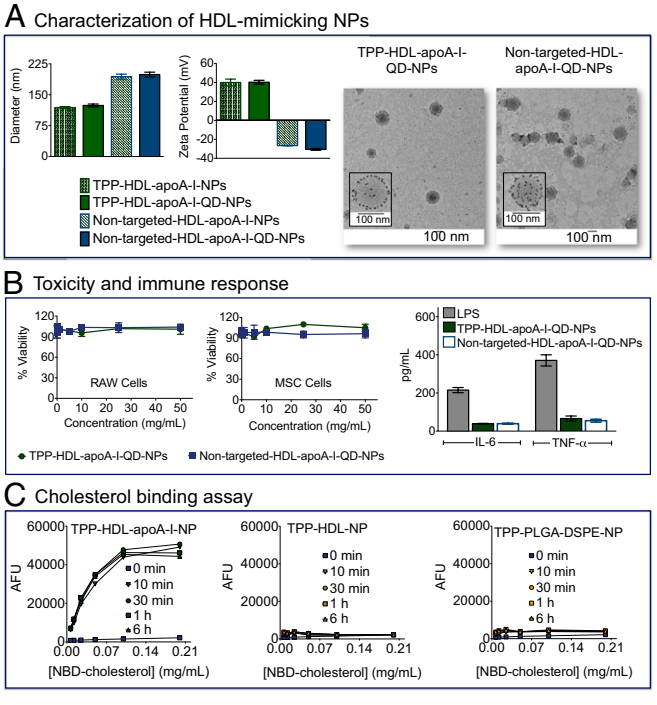


**Fig. 2.** (*A*) Size and zeta potential of targeted and nontargeted HDL-mimicking NPs with or without QD (*Left*) and TEM images of targeted and nontargeted QD-loaded HDL-mimicking NPs (*Right*). (*B*) Toxicity profiles of targeted and nontargeted HDL-mimicking NPs in RAW macrophages and MSC cells as determined by MTT assay (*Left* and *Center*) and secretion of IL-6 and TNF-α from RAW 264.7 macrophages with targeted and nontargeted NPs (0.5 mg/mL) after 12 h (*Right*). (*C*) Binding of NBD cholesterol to TPP-HDL-apoA-I NPs (*Left*). TPP-HDL NPs (*Center*) and TPP-PLGA-DSPE NPs (*Right*) were used as controls.

was used as a positive control. Incubation of Raschke, Ralph, Watson (RAW) 264.7 macrophages with targeted and nontargeted HDL NPs (0.5 mg/mL) did not show secretion of IL-6 and TNF-α (Fig. 2*B*). After seeing that these NPs have no proinflammatory effect on naïve macrophages, the ability of the targeted and nontargeted NPs to modulate cytokine production in LPS-activated RAW macrophages was assessed. When exposed to an optimal concentration of LPS (100 ng/mL) for 24 h, macrophages produce enhanced amounts of IL-6 and TNF-α (*SI Appendix*, Fig. S8). Treatment of these LPS-activated macrophages with targeted or nontargeted NPs (0.5 mg/mL with respect to total NP) for 12 h did not show any additional amounts of IL-6 and TNF-α; a slight decreased production of both the cytokines was observed in the presence of these NPs (*SI Appendix*, Fig. S8). This observation further confirms that these NPs have no effect on naïve and M1-polarized macrophages. Targeted and nontargeted HDL-NP–induced cytotoxicity was assessed by the 3-(4,5-dimethylthiazol-2-yl)-2,5-diphenyltetrazolium bromide (MTT) assay in RAW macrophages and primary human mesenchymal stem cells (MSCs). MSCs represent an interesting target cell type regarding nanotoxicology and especially nanogenotoxicology because they actively proliferate and repeatedly expand in contrast to other primary cells, although they are not immortalized. Directly following 72 h incubation with NPs at various concentrations showed no particle-related cytotoxicity and morphological transformation even at 50 mg/mL concentration compared with that of untreated cells (Fig. 2*B*). The use of biodegradable components in this HDL-mimicking NPs resulted in a biocompatible, nontoxic, and nonimmunogenic formulation.

**In Vitro Cholesterol Binding Properties.** A fluorescent sterol, NBD cholesterol or 22-(*N*-(7-nitrobenz-2-oxa-1,3-diazo-4-yl)-amino)-23,24-bisnor-5-cholen-3β-ol was used to examine the HDL-mimicking NP-mediated cholesterol uptake to explore the therapeutic potential. The weak fluorescence of NBD cholesterol in polar environment was enhanced by the presence of nonpolar TPP-HDL-apoA-I-NP matrix (Fig. 2*C*). Similar formulation without any apoA-I, TPP-HDL NPs, did not show any cholesterol binding. Control polymer lipid hybrid NPs prepared from PLGA-COOH, DSPE-PEG-COOH, and stearyl-TPP; PLGA-DSPE NPs, which lack HDL-apoA-I mimicking core, did not show cholesterol binding properties. We also explored time and temperature-dependent cholesterol binding abilities of the targeted NPs. Storage of targeted NPs at 4 °C, RT, and 37 °C in 10% FBS-DMEM and examination of NBD-cholesterol binding for 7-d at all three temperatures indicated enhanced cholesterol binding with the NPs that were kept at RT or at 37 °C compared with those at 4 °C (*SI Appendix*, Fig. S9). We think this is due to increased NP swelling at higher temperatures. A decreased cholesterol-binding trend with time indicates biodegradable nature of these NPs. These preliminary experiments are indicative that cholesterol can bind to TPP-HDL-apoA-I NPs for potential participation in the RCT pathway.

**$\Delta\psi_m$-Targeted TPP-HDL-apoA-I-QD NPs Located in the Mitochondria.** Significant cell association and mitochondrial internalization of the targeted TPP-HDL-apoA-I-QD NPs by healthy RAW 264.7 was noted (Fig. 3*A*). Only limited nonspecific cytosolic uptake was observed for the nontargeted HDL-apoA-I-QD NPs (Fig. 3*A*). To find out whether the uptake of the targeted NPs is a $\Delta\psi_m$-driven process, studies were performed in the presence of a mild uncoupler carbonylcyanide-*p*-(trifluoromethoxy)phenylhydrazone (FCCP) (Fig. 3*B*). Uptake of TPP-HDL-apoA-I-QD NPs were completely blocked by the presence of FCCP, which abolishes the $\Delta\psi_m$ of the inner mitochondrial membrane (IMM), as shown by in vivo imaging system (IVIS) analyses of the mitochondrial and cytosolic fractions of the NP-treated cells in the absence or presence of the uncoupler FCCP (Fig. 3*B*). The mitochondrial uncoupler FCCP had no effect on the uptake profile of nontargeted NPs (*SI Appendix*, Fig. S10). These observations were further confirmed by determining the QD content of the mitochondrial and cytosolic fractions of the FCCP-treated macrophages, which showed no significant accumulation of the targeted NPs in the mitochondria of $\Delta\psi_m$-blocked macrophages. Taken together, these data support our claim that the TPP-HDL-apoA-I NPs takes advantage of the substantial negative $\Delta\psi_m$ maintained across the IMM at crossing the hydrophobic membranes and preferentially associate with the mitochondrial network. To further determine the localization of the targeted HDL-apoA-I NPs within these organelles, targeted NP-treated RAW macrophage mitochondrial fractions were lysed and further fractionated into outer mitochondrial membrane (OMM), IMM, innermembrane space, and mitochondrial matrix. These fractions were examined by IVIS analyses and ICP-MS (Fig. 3*C*). Within the mitochondria, TPP-HDL-apoA-I-QD NPs were localized mainly in the mitochondrial matrix and the innermembrane space as demonstrated by IVIS analyses (Fig. 3*C*). This observation was further supported by quantitative ICP-MS of targeted NP-treated mitochondrial subfractions. Cadmium (Cd) quantification of mitochondrial compartments demonstrated that targeted NPs were mainly found in the mitochondrial matrix ($22.7 \pm 0.9\%$) and the innermembrane space ($12.6 \pm 0.4\%$); only trace amounts of these NPs were detected in the IMM ($2.3 \pm 0.1\%$) or the OMM ($0.1 \pm 0.04\%$). In our study, isolation of mitochondrial compartments and analyses using IVIS and ICP-MS provided us concrete evidence that our targeted HDL NPs reside inside the mitochondrial matrix. Our data also suggest that these targeted NPs are imported to the matrix by an $\Delta\psi_m$-mediated mechanism that is active only in healthy cells with active mitochondria. These targeted NPs will take the advantage of collapse of $\Delta\psi_m$ during apoptotic events of macrophages for selective detection of vulnerable plaques.

**Apoptosis Sensing in Macrophages.** Apoptosis-sensing ability of this platform was investigated in apoptotic RAW macrophages by fluorescence microscopy, flow cytometry, IVIS, and ICP-MS analyses.

The permanent collapse of the $\Delta\psi_m$ plays a key role in apoptosis. Because of its apparent simplicity, we carried out a qualitative fluorescence imaging of $\Delta\psi_m$ collapse for monitoring apoptotic event by using macrophages. During apoptosis, changes in the $\Delta\psi_m$ occur because of the opening of the mitochondrial permeability transition pore. The electrochemical proton gradient across the IMM in viable cells favors inward movement of TPP-HDL-apoA-I-QD NPs into the mitochondrial matrix (Fig. 3). Apoptotic macrophages treated with this NP showed a significant decrease in NP accumulation due to the lost gradient early on induction of apoptosis (Fig. 4*A*) compared with the healthy cells. Therefore, these NPs manifest signal reduction on induction of the macrophage death process, in contrast to the nontargeted NPs, which do not show any significant difference between viable and apoptotic cells (Fig. 4*A*).

Qualitative detection of apoptotic macrophages using our targeted NPs was further supported quantitatively by carrying out flow cytometry. Annexin V, which is used for noninvasive apoptosis detection in myocardial infarction and inflammatory myocardial diseases (20), was used as a control. By using a low concentration of TPP-HDL-apoA-I-QD NPs, significant detection of apoptotic macrophages was observed (Fig. 4*B*) that was comparable to annexin V (*SI Appendix*, Fig. S11). In the flow cytometric profiles, apoptotic cells were recognized by the targeted NPs on the basis of well-established light scattering characteristics. The electrochemical proton gradient across the IMM in viable cells favors association of the targeted NPs with the mitochondria. This gradient is lost with an overall reduction in the concentration of the targeted NPs in the apoptotic cells (Fig. 4*B*). Nontargeted NPs, in contrast, did not exhibit resolution between apoptotic and nonapoptotic cells (Fig. 4*B*). Thus, these data support the hypothesis that mitochondrial demise step can be used as an indicator by the targeted HDL NPs to differentiate between vulnerable and stable plaques.

To confirm the apoptosis-sensing property further, we fractionated the NP-treated apoptotic and healthy cells to mitochondrial

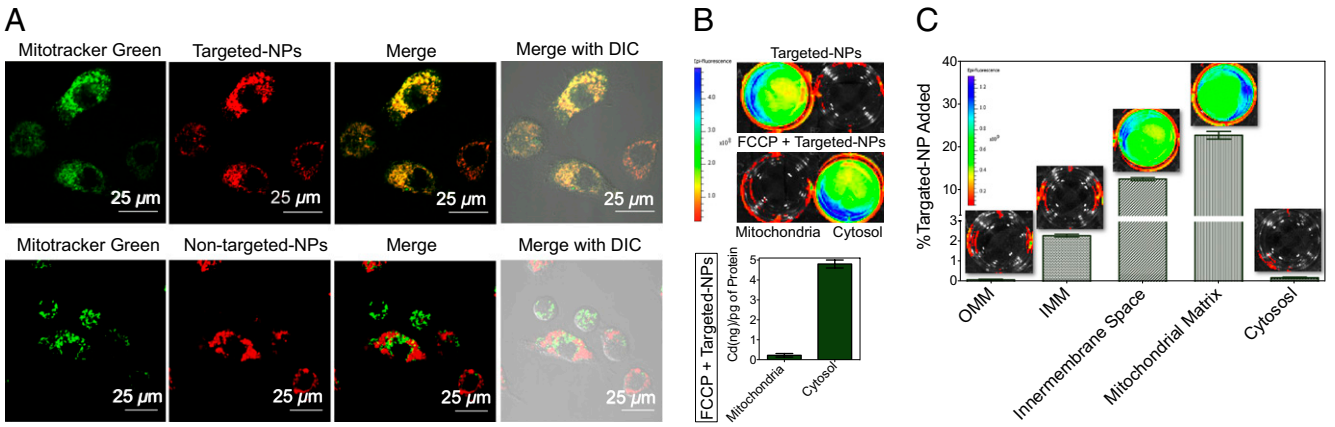


**Fig. 3.** (*A*) Subcellular localization of TPP-HDL-apoA-I-QD NPs and nontargeted HDL-apoA-I-QD NPs in RAW macrophages. RAW 264.7 cells were exposed to targeted NPs (diameter, 125 nm; zeta potential, 37 mV) and nontargeted NPs (diameter, 189 nm; zeta potential, −29 mV) at 270 μM (with respect to cholesterol) for 4 h. They were stained with the mitochondrial marker MitoTracker Green, and live cell imaging was performed. The merged images show effective association of the targeted NPs (red) with the mitochondria (green), and no significant association was observed with nontargeted NPs. (*B*) IVIS of mitochondrial and cytosolic fractions of RAW macrophages after treatment with targeted TPP-HDL-apoA-I-QD NPs with or without collapse of $\Delta\psi_m$ by addition of FCCP. QD content in the mitochondrial and cytosolic fractions of FCCP-blocked cells by ICP-MS. (*C*) Quantification of targeted NPs in the mitochondrial subfractions by ICP-MS and IVIS.

and cytosolic fractions and conducted IVIS (Fig. 4*C*). We expected in the healthy cells with respiration-active mitochondria that the targeted TPP-HDL-apoA-I-QD NPs will localize in the mitochondria, whereas the nontargeted NPs will accumulate in the cytosols. In apoptotic cells, upon collapse of $\Delta\psi_m$, the targeted NPs will get expelled out to the cytosols with an overall reduced uptake. Upon apoptosis, we observed loss of fluorescence in the mitochondrial fractions with the targeted TPP-HDL-apoA-I-QD NPs, whereas, the nontargeted NPs did not show any difference between healthy and apoptotic cells (Fig. 4*C*). Quantifying Cd by ICP-MS in the mitochondrial and cytosolic fractions further supported that the targeted HDL NPs have the superior ability to sense apoptosis in macrophages (Fig. 4*C*). Compared with the transient nature of PS externalization used by labeled annexin V to detect apoptosis associated with unstable human carotid plaques (21), loss of $\Delta\psi_m$ used by our targeted NPs is an ongoing process (22) and, hence, allows detection not limited to a specific time window. The potential toxic effects of QDs should be considered for possible in vivo translation of this technology (23). However, we want to emphasize that the biodegradable polymer-conjugated PLGA-*b*-PEG-QDs as used in our studies can be better suited for in vivo studies. For polymer-conjugated QDs, chemical and enzymatic degradation of the QD core will be less compared with the traditional QDs. Polymer-conjugated QDs embedded in the NP core will have the potential to show in vivo clearance by slow infiltration and excretion. With QD toxicity issues and the limitations of optical imaging in the clinic, we think that this highly sensitive HDL-based NP could provide a platform for preclinical drug screening and therapy monitoring. In the future, scientists should use a complementary magnetic resonance imaging (MRI) by incorporating iron oxide for

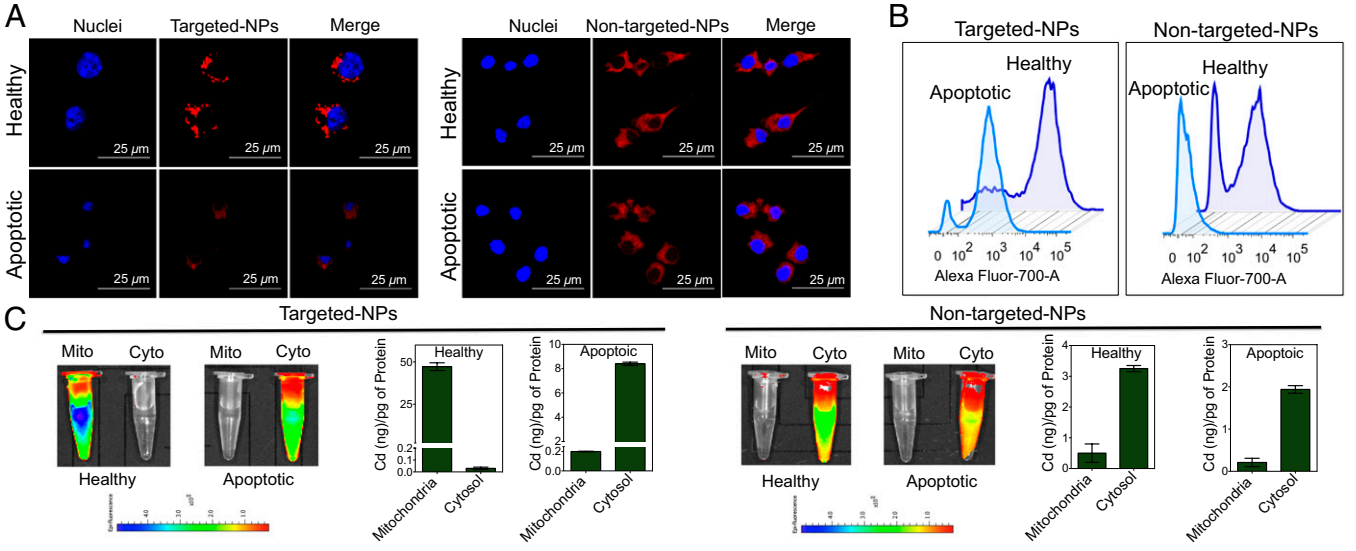


**Fig. 4.** (*A*) Apoptosis detection by HDL-apoA-I-QD NPs in RAW macrophages by confocal microscopy. Apoptosis was induced by treating macrophages with etoposide. The medium was changed and targeted, and nontargeted NPs were added. Cells were fixed, and nuclei were stained with Hoechst and visualized by confocal microscopy. (*B*) Flow cytometry patterns of RAW macrophages treated with the targeted and nontargeted NPs with or without etoposide. Macrophage monolayers were incubated for 3 h with TPP-HDL-apoA-I-QD NPs (*Left*) or nontargeted-HDL-apoA-I-QD NPs (*Right*). Before NP treatment, apoptosis was induced by using the above-mentioned conditions. Histograms depict all of the acquired events. (*C*) IVIS and ICP-MS analysis of mitochondrial and cytosolic fractions of healthy and apoptotic RAW macrophages after treatment with targeted (*Left*) and nontargeted NPs (*Right*).

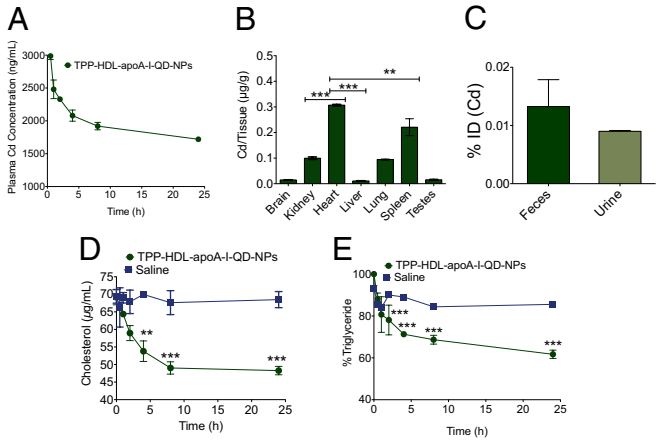


**Fig. 5.** (*A*) Variation of Cd concentration (ng/mL) in plasma with time following the administration of targeted TPP-HDL-apoA-I-QD NPs i.v. to rat. (*B*) Tissue distribution of targeted TPP-HDL-apoA-I-QD NPs in male rats. (*C*) Cumulative 24-h excretion of TPP-HDL-apoA-I-QD NPs in male rats. Changes in levels of plasma total cholesterol (*D*) and triglyceride (*E*) in rats administered with TPP-HDL-apoA-I-QD NPs. Statistical analyses were performed by using one-way ANOVA with Tukey post hoc test. $^{**}P < 0.001$, $^{***}P < 0.0001$.

in vivo imaging and use ex vivo QD imaging to complement the MRI results.

**BioD and PK of Targeted TPP-HDL-apoA-I NPs.** Favorable BioD, excretion, and PK properties are important for a newly developed NP platform for its in vivo application. To determine the PK, bioD, and excretion profiles, we injected TPP-HDL-apoA-I-QD NPs into Sprague–Dawley rats by a single dose i.v. injection; blood samples at predetermined time points up to 24 h after injection, organs after 24 h, and cumulative urine and feces over 24 h were collected. Analyses of the plasma samples for Cd by ICP-MS and calculation of PK parameters by a two-compartment i.v. input model revealed a plasma elimination half life ($t_{1/2}$) from the central compartment of ∼36 min (Fig. 5 and Table 1). This initial phase is followed by a slower decline, a very high $t_{1/2}$ value in the periphery compartment of ∼72 h was observed (Table 1). Such a slow clearance of this engineered NP indicates that this platform has the potential to serve as an excellent delivery system. The total body clearance ($C_L$) of the targeted HDL-mimicking NPs was 0.03 mL/h. The longer terminal phase $t_{1/2}$ and a smaller $C_L$ of the targeted NPs indicate that the engineered HDL-mimicking NPs could stay in the body for a longer period (Table 1). Based on the very high area under curve (AUC) of 47,196 ng/mL and peak plasma concentration ($C_{max}$) of 3,676 ng/mL produced by the HDL-mimicking NPs indicate that these NPs are delivered into the bloodstream very effectively (Table 1). The extraordinary PK properties of our HDL NPs mimic various attractive features of native HDL such as long circulation, $t_{1/2}$ ranging from 10 to 12 h in rodents and 5 d in humans due to the presence of unique combination of apoA-I, lipid, and favorable surface properties (24). A smaller volume of distribution ($V_d$) was observed in the rats receiving the targeted NPs (Table 1). It is possible that upon i.v. administration these NPs, because of their unique composition, may hinder the distribution in the body or rapid conversion to metabolites.

The excretion profiles for the HDL mimicking NPs via urine and feces were studied by measuring Cd levels from QDs (Fig. 5). At 24 h after injection, cumulative NPs recovered in urine and feces represented only 0.009% and 0.013% of the administered dose, respectively (Fig. 5).

The concentration of the targeted HDL-mimicking NPs was monitored in major tissues, including spleen, liver, lungs, brain, heart, kidneys, and testes at 24 h after dose (Fig. 5). The total recovery in organs accounted for ∼4.8% of the dose administered with the highest accumulation in the heart (Fig. 5). Quantitative ICP-MS results indicated that 1.5% of the injected dose of our engineered NPs was distributed in the heart after 24 h. In general, positively charged NPs accumulate in the liver and the spleen because of the positive zeta potential, which favors uptake by phagocytic cells of the reticuloendothelial system mainly present in these organs. The targeted HDL-mimicking NPs despite positively charged surface showed a very high heart-to-liver ratio of 29 and a moderate heart-to-spleen ratio of ∼1.5 (Fig. 5). The targeted NPs also showed a high heart-to-kidney ratio of ∼3. The absence of TPP-HDL-apoA-I-QD NPs in the lungs as indicated by the high heart-to-lung ratio of ∼3.5 reflects a satisfactory colloidal stability of these NPs despite the presence of negatively charged serum proteins, which are well known for inducing the agglomeration of positively charged NPs. Such a colloidal stability can probably be originated because of the steric hindrance caused by the TPP moieties on the surface of the NPs. We believe that NP distribution in the heart is due to high NP concentration (57% of the injected dose) in the circulatory system, which increases the possibility that the NPs accumulate in the heart. Significant accumulation of the targeted HDL-mimicking NPs in the heart indicates that these NPs have the potential for further development for imaging and therapy of CHD.

**In Vivo Lipid Dynamics by TPP-HDL-apoA-I NPs.** Studies have shown an inverse correlation between plasma HDL concentrations and atherosclerotic cardiovascular risk (25). HDL and apoA-I play key roles in RCT from atherosclerotic plaques to the liver. Cholesterol in the nascent discoidal HDL is esterified by lecithin-cholesterol acyltransferase to form cholesteryl esters, which occupies the core of HDL, thus producing a steady gradient of free cholesterol and enabling HDL to accept cholesterol from various donors. We speculated that the HDL-mimicking NPs with a CE core would be able to mimic the RCT action of natural HDL. In our study, targeted TPP-HDL-apoA-I-QD NPs significantly reduced the serum total cholesterol and triglyceride compared with the saline control (Fig. 5 *D* and *E*). TPP-HDL-apoA-I-QD NPs in low dose (80 $\mu g \cdot kg^{-1}$ with respect to QD, 10 $mg \cdot kg^{-1}$ with respect to total NP) for 24 h tended to decrease total cholesterol levels by 30% ($P < 0.0001$) (Fig. 5*D*) and triglyceride levels by 24% ($P < 0.0001$) (Fig. 5*E*) compared with the saline group. These effects are likely to be related to the binding of cholesterol to TPP-HDL-apoA-I NPs as seen in our in vitro cholesterol-binding experiments (Fig. 2*C*). It is important to note that these data demonstrate potential utility of this engineered HDL-mimicking NP as a therapeutic platform for atherosclerosis. Given the simplicity of the system, biodegradability, and the scope of easy manipulation, this platform has the potential for further development to improve the lipid profile for dyslipidemic patients.

**Table 1. PK parameters of TPP-HDL-apoA-I-QD NPs by using two-compartment model**

| PK parameter | Values |
|---|---|
| $AUC_{[0\text{-}24\ h]}$,* h.ng/mL | 47,196 |
| $C_{max}$,* ng/mL | 3,676 |
| Central compartment (initial phase, $t = 0$) | |
| $V_d$, mL/kg | 21.5 |
| $C_L$ at $t = 0$, mL/h | 3.5 |
| $t_{1/2}$, h | 0.6 |
| Periphery compartment (terminal phase, $t = 24$ h) | |
| $V_d$, mL/kg | 9.9 |
| $C_L$, terminal, mL/h | 0.03 |
| $t_{1/2}$, h | 71.7 |

Least-square fit to model. $C = a \times \exp[(-k_1 \times t) + b \times \exp(-k_2 \times t)]$. AUC, area under curve; $C_{max}$, Peak plasma concentration; $C_L$, total body clearance; $t_{1/2}$, plasma half-life; $V_d$, volume of distribution.
*Model used to extrapolate concentrations at $t = 0$.

A proof-of-concept demonstration of a biodegradable polymer lipid hybrid synthetic HDL-mimicking NP was established for imaging and therapy of vulnerable plaques. We demonstrated that the mitochondria-targeted NPs can sense apoptosis with high resolution over the nontargeted NPs. These NPs closely mimic endogenous HDL in cholesterol-binding properties. In addition, we observed the avid uptake of the targeted HDL NPs by the mitochondria of macrophages. In vivo applicability of the targeted-HDL NPs for imaging and therapy of atherosclerosis was demonstrated by establishing that this system is nontoxic, shows promising PK parameters and favorable bioD, and has the ability to reduce lipid levels. Understanding of this biodegradable HDL-NP mimic could lead to the development of candidates that can detect vulnerable plaque early and enhance atheroprotection by increasing levels of HDL and/or enhancing its functionality. Although additional studies should address the applicability of this platform for imaging and therapy of CHD, this proof-of-concept study demonstrates the feasibility, flexibility, and ease with which the composition of this platform can be manipulated or modified to make them well suited for the creation of artificial HDL-based biodegradable NPs for imaging and therapy of atherosclerosis.

## Materials and Methods

**Materials.** Description of materials can be found in *SI Appendix*.

**Animals.** Animals were obtained from Harlan Laboratory and handled in accordance with The Guide for the Care and Use of Laboratory Animals of American Association for Accreditation of Laboratory Animal Care (AAALAC), Animal Welfare Act (AWA), and other applicable federal and state guideline. All animal work presented here was approved by Institutional Animal Care and Use Committee (IACUC) of University of Georgia.

**Synthesis of HDL-Mimicking NPs.** Targeted hybrid NPs were prepared via self-assembly of PLGA, PLGA-*b*-PEG-QD, CO, stearyl-TPP, DSPE-PEG-COOH, and apoA-I mimetic 4F peptide through a modified nanoprecipitation method as described in *SI Appendix*, Fig. S4. NP size (diameter, nanometers), PDI, and surface charge (zeta potential, millivolts) were obtained from three independent measurements with a Zetasizer Nano-ZS DLS detector (*SI Appendix*, Figs. S5 and S6). QD loading in the NPs was quantified by ICP-MS, and apoA-I loading was determined by following tryptophan absorbance at 280 nm. The amount of cholesterol was determined by an AmplexRed assay. Reproducibility of construction of targeted and nontargeted HDL-mimicking NPs was confirmed by multiple independent nanoprecipitation experiments (*SI Appendix*, Table S2).

**Cholesterol-Binding Experiments.** Cholesterol binding to TPP-HDL-apoA-I NPs, TPP-HDL NPs, and TPP-PLGA-DSPE NPs was performed by using procedures described in *SI Appendix*.

**Imaging Intracellular Fractions of Apoptotic and Healthy Cells by IVIS.** Targeted or nontargeted NP-treated intracellular fractions of RAW macrophages were isolated by using procedures described in *SI Appendix*. The mitochondrial and cytosolic fractions were imaged.

**Mitochondrial Subfractionation.** TPP-HDL-apoA-I-QD NPs (0.5 mg/mL) were internalized in RAW 264.7 macrophages for 12 h. The mitochondria and the cytosol were isolated by using a mitochondria isolation kit for mammalian cells, and the fractions were further subfractionated by using a modified literature reported protocol as described in *SI Appendix* (26).

**BioD and PK Studies.** BioD and PK of TPP-HDL-apoA-I-QD NPs were determined by using male Sprague–Dawley rats. Details about bioD-PK study used can be found in *SI Appendix*.

**Blood Plasma Cholesterol and Triglyceride Quantification.** Cholesterol and triglyceride contents in blood plasma were quantified by AmplexRed and AdipoRed assays, respectively as described in *SI Appendix*.

**Statistics.** Statistical analyses were performed by using GraphPad Prism software version 5.00 (GraphPad Software). Comparisons between two values were performed by using an unpaired Student *t* test. A one-way ANOVA with a post hoc Tukey test was used to identify significant differences among the groups.

**ACKNOWLEDGMENTS.** We thank Dr. Nagesh Kolishetti for helpful discussions and Walter J. Lunsmann (VivoPath) and Dr. Angel Padilla for assistance with PK parameter calculations and IVIS, respectively. This work was supported by the National Institutes of Health Startup Grant P30GM092378 and by the Office of the Vice President for Research, University of Georgia (to S.D.).

1. Sanz J, Fayad ZA (2008) Imaging of atherosclerotic cardiovascular disease. *Nature* 451(7181):953–957.
2. Ross R (1993) The pathogenesis of atherosclerosis: A perspective for the 1990s. *Nature* 362(6423):801–809.
3. van der Velde AE (2010) Reverse cholesterol transport: From classical view to new insights. *World J Gastroenterol* 16(47):5908–5915.
4. Ross R, Glomset JA (1973) Atherosclerosis and the arterial smooth muscle cell: Proliferation of smooth muscle is a key event in the genesis of the lesions of atherosclerosis. *Science* 180(4093):1332–1339.
5. Desai MY, Schoenhagen P (2009) Emergence of targeted molecular imaging in atherosclerotic cardiovascular disease. *Expert Rev Cardiovasc Ther* 7(2):197–203.
6. Group TBS (2000) Secondary prevention by raising HDL cholesterol and reducing triglycerides in patients with coronary artery disease: The Bezafibrate Infarction Prevention (BIP) study. *Circulation* 102(1):21–27.
7. Kruth HS (2001) Macrophage foam cells and atherosclerosis. *Front Biosci* 6: D429–D455.
8. Petit PX, et al. (1995) Alterations in mitochondrial structure and function are early events of dexamethasone-induced thymocyte apoptosis. *J Cell Biol* 130(1):157–167.
9. Frias JC, Williams KJ, Fisher EA, Fayad ZA (2004) Recombinant HDL-like nanoparticles: A specific contrast agent for MRI of atherosclerotic plaques. *J Am Chem Soc* 126(50): 16316–16317.
10. Skajaa T, et al. (2010) High-density lipoprotein-based contrast agents for multimodal imaging of atherosclerosis. *Arterioscler Thromb Vasc Biol* 30(2):169–176.
11. Frias JC, Ma Y, Williams KJ, Fayad ZA, Fisher EA (2006) Properties of a versatile nanoparticle platform contrast agent to image and characterize atherosclerotic plaques by magnetic resonance imaging. *Nano Lett* 6(10):2220–2224.
12. Yang M, et al. (2011) Efficient cytosolic delivery of siRNA using HDL-mimicking nanoparticles. *Small* 7(5):568–573.
13. Zhang Z, et al. (2010) HDL-mimicking peptide-lipid nanoparticles with improved tumor targeting. *Small* 6(3):430–437.
14. McMahon KM, et al. (2011) Biomimetic high density lipoprotein nanoparticles for nucleic acid delivery. *Nano Lett* 11(3):1208–1214.
15. Thaxton CS, Daniel WL, Giljohann DA, Thomas AD, Mirkin CA (2009) Templated spherical high density lipoprotein nanoparticles. *J Am Chem Soc* 131(4):1384–1385.
16. Yang S, et al. (2013) Biomimetic, synthetic HDL nanostructures for lymphoma. *Proc Natl Acad Sci USA* 110(7):2511–2516.
17. Smith RA, Porteous CM, Gane AM, Murphy MP (2003) Delivery of bioactive molecules to mitochondria in vivo. *Proc Natl Acad Sci USA* 100(9):5407–5412.
18. Marrache S, Dhar S (2012) Engineering of blended nanoparticle platform for delivery of mitochondria-acting therapeutics. *Proc Natl Acad Sci USA* 109(40):16288–16293.
19. Kontush A, Chapman MJ (2006) Functionally defective high-density lipoprotein: A new therapeutic target at the crossroads of dyslipidemia, inflammation, and atherosclerosis. *Pharmacol Rev* 58(3):342–374.
20. Flotats A, Carrió I (2003) Non-invasive in vivo imaging of myocardial apoptosis and necrosis. *Eur J Nucl Med Mol Imaging* 30(4):615–630.
21. Kietselaer BLJH, et al. (2004) Noninvasive detection of plaque instability with use of radiolabeled annexin A5 in patients with carotid-artery atherosclerosis. *N Engl J Med* 350(14):1472–1473.
22. Green DR, Kroemer G (2004) The pathophysiology of mitochondrial cell death. *Science* 305(5684):626–629.
23. Fitzpatrick JA, et al. (2009) Long-term persistence and spectral blue shifting of quantum dots in vivo. *Nano Lett* 9(7):2736–2741.
24. Daerr WH, Pethke W, Windler ETE, Greten H (1990) Biotinyl-high-density lipoproteins as a probe for the determination of high-density lipoprotein turnover in humans. *Biochim Biophys Acta* 1043(3):311–317.
25. Boden WE (2000) High-density lipoprotein cholesterol as an independent risk factor in cardiovascular disease: Assessing the data from Framingham to the Veterans Affairs High—Density Lipoprotein Intervention Trial. *Am J Cardiol* 86(12A):19L–22L.
26. Benga G, et al. (1979) Fractionation of human liver mitochondria: Enzymic and morphological characterization of the inner and outer membranes as compared to rat liver mitochondria. *J Cell Sci* 35:417–429.